Received: 27 October 2017 | Accepted: 11 December 2017

DOI: 10.1111/jace.15383

ORIGINAL ARTICLE

Journal of the American Ceramic Society

Hard boron rich boron nitride nanoglasses

Ayşegül Ö. Çetin | **Murat Durandurdu**

Department of Materials Science & Nanotechnology Engineering, Material Science & Mechanical Engineering Program, Abdullah Gül University, Kayseri, Turkey

Correspondence
Murat Durandurdu, Department of Materials Science & Nanotechnology Engineering, and Material Science & Mechanical Engineering Program, Abdullah Gül University, Kayseri, Turkey.
Email: murat.durandurdu@agu.edu.tr

Funding information
Scientific and Technological Research Council of Turkey, Grant/Award Number: 114C100

Abstract

Boron-rich amorphous boron nitride (B_xN_{1-x}, $0.55 \leq x \leq 0.95$) alloys are generated by means of ab initio molecular dynamics simulations and their local structure, mechanical properties and electronic structure are exposed. BN:B phase separations are perceived in all amorphous networks, suggesting that these materials can serve as *nanoglass* ceramics. The sp^2 hybridization is the main building unit in the BN-rich regions for low boron concentrations, and the models carry locally the signature of the two-dimensional hexagonal BN structure. The amorphous states having both sp^2 and sp^3 hybridizations form for boron contents between 70% and 80%. At higher boron concentrations, sp^3 hybridization with a fraction of ~90%-98% is detected as seen in the cubic or wurtize BN crystals. In the boron rich regions, the ideal and defective pentagonal pyramids emerge at 60% boron content, and the first complete B_{12} molecule develops at 70% boron concentration. In addition to the B_{12} icosahedron, the formation of a cage-like B_{16} molecule is, for the first time, discovered in some amorphous alloys. The isolated B_{16} molecule is, however, found to be unstable. The Vickers harness calculations reveal that some of these amorphous alloys can serve as hard materials. When their electron properties are considered, all amorphous materials are predicted to be semiconducting.

KEYWORDS

B_{16} molecule, boron nitride, boron rich, hard materials, nanoglass

1 | INTRODUCTION

Boron Nitride (BN) is an important ceramic and has received considerable attentions due to its excellent optical, electrical, and mechanical properties such as high thermal conductivity, high strength, high temperature stability, low dielectric constant, wide band gap, n- and p-type dupability, lubricity, the capability of hydrogen uptake, etc.[1-16] Therefore, it has various advanced technological applications ranging from cosmetic products to flexible nanoelectronics.

BN was first synthesized in the form of a hexagonal structure (h-BN) in 1840.[17] Being a two-dimensional (2D) layered structure with sp^2 hybridization, it is the most stable form at ambient conditions. Another well-known 2D structured BN has the rhombohedral symmetry (r-BN).[18] The high temperature and pressure treatments of h-BN and r-BN yield three-dimensional (3D) zinc-blende cubic (c-BN) and/or wurtzite (w-BN) structures having sp^3 hybridization.[19-35] Both BN phases are considered as superhard materials.

Boron (B) rich nitrides are new materials of interest and possess high hardness, and high thermal and chemical stabilities. Therefore, they can be used in advanced electronics as well.[13,36] Several B subnitrides such as $B_{13}N_2$, $B_{50}N_2$, B_6N, B_4N, etc.[13,36-41] have been proposed to date. They

have been commonly synthesized under the high-pressure treatments of B/BN melts. The structure and/or thermodynamic stability of some of these B subnitrides have not been well established yet. The $B_{13}N_2$ and $B_{50}N_2$ phases have a 3D structure and are believed to consist of distorted B_{12} icosahedrons connected by N–B–N atomic chains, and inter-icosahedral B–B bonds.[13,36,38,39] The existence of B_6N still remains mystery.[42]

Amorphous BN (a-BN) is another interesting form of BN and can be prepared using different experimental techniques such as ball milling technique, very high frequency plasma chemical vapor deposition, etc.[43,44] The short-range order of a-BN is predominantly due to sp^2 hybridization.[43-45] It consists of randomly oriented h-BN-like nanosheets and it is almost free from chemical disorder (no homopolar bonds).[45]

B-rich a-BN or hydrogenated B-rich a-BN materials are of interest as well and have been investigated in several experiments.[11,46-48] Yet most of these studies primarily focused on their physical properties, in particular, their electronic structures and did not provide solid information about their short-range order and some of their mechanical properties in details. On the basis of the X-ray diffraction spectra,[47] different local structures were proposed for B-rich a-BN depending on B content. For high B concentrations, the amorphous materials were predicted to have a random network of icosahedra. For the films with B contents less than 80 at.%, the icosahedrons were separated and the h-BN like structure was emerged.[47]

In this work, we use ab initio molecular dynamics simulations to model B-rich B_xN_{1-x} $(0.55 \leq x \leq 0.95)$ amorphous materials and to explore their local structure, electronic structure and mechanical properties. We reveal, for the first time, some remarkable features of these amorphous systems. The observation of B:BN phase separations, a content-induced structural phase transformation in the BN-rich domains, the formation of a cage-like B_{16} molecule, high hardness of some amorphous alloys are important outcomes of this study.

2 | COMPUTATIONAL METHOD

All simulations were performed by the SIESTA density functional theory (DFT) code.[49] We used the Becke gradient exchange functional[50] and Lee, Yang, and Parr correlation functional[51] to evaluate the exchange correlation energy and the Troullier and Martins approach to construct norm-conserving nonlocal pseudopotentials.[52] The simulations were done at Γ points using the DZP basis. We set the time step of each molecular dynamics simulation 1.0 fs. We adopted the structure of liquid $B_{0.5}N_{0.5}$ having 216 atoms (108 N and 108 B) at 3300 K[45] as a starting structure and substituted randomly N atom by B atom until we had a certain amount of B concentration (~55%-95%). The initial configurations were subjected to high temperatures and thermalized at 2500 K (~95 at% B)-3300 K (~55 at% B) for at least 50.0 ps and then they were quenched to 300 K in ~150.0-300.0 ps. All these simulations were performed within the NPT (isothermal-isobaric) ensemble. We applied the velocity scaling method and the Parrinelo-Rahman technique[53] to control temperature and pressure, respectively. Yet during the thermalization and quenching procedures, no shear deformations were allowed. The resulting models at 300 K were optimized, using the NPH (isobaric-isenthalpic) ensemble until the maximum force is less than 0.02 eV/Å. The VESTA[54] and ISAACS[55] programs were used to visualize and analyze the amorphous models, separately.

3 | RESULTS

3.1 | Structural properties

In order to understand the nature of bonding for each atomic species and to identify the microstructure of the amorphous configurations, we primarily study their partial pair distribution functions (PPDFs) and present some of them in Figure 1. The PPDFs exhibit the typical characteristics of an amorphous network for all compositions such that they have a well-defined first neighbor peak and the lack of long-range correlations. As predictable, we observe drastic changes in the distributions with increasing boron concentration: the intensity of the first B–B peak increases slowly while that of the second B–B peak decreases. Figure 2 shows the variation in the first peak position of the B–N, B–B and N–N correlations as a function of B concentration. The average B–N bond distance is projected to be 1.43 Å at 55% B content, which is indeed pretty close to the sp^2 bond length of 1.44 Å reported for h-BN.[56] The B-N bond separation remains almost unchanged up to 70 at. % B at which point it begins to rise and reaches a value of 1.53 Å at 80% B content. After this concentration, it exhibits a small fluctuation around this value. It should be noteworthy here that the mean B–N bond separation (1.53 Å) at 80% and higher B concentrations is rather parallel to the sp^3 bond distance of 1.54 Å reported for c-BN.[56] The first peak of the B-B bond correlation with 55 at.% B is located at 1.67 Å and increases progressively to a value of ~1.77 Å up to 80 at.% B. After which, it remains almost null. The B–B bond length, ~1.77 Å, is relatively comparable with 1.78-1.80 Å formed in the liquid B and a-B.[57,58] In the model having 55 at.% B, the N–N distance is positioned at 2.50 Å. This value is pretty close to the N–N separation of 2.50 Å originated in h-BN[56] and 2.56 Å found in c-BN.[56] With increasing B content, the

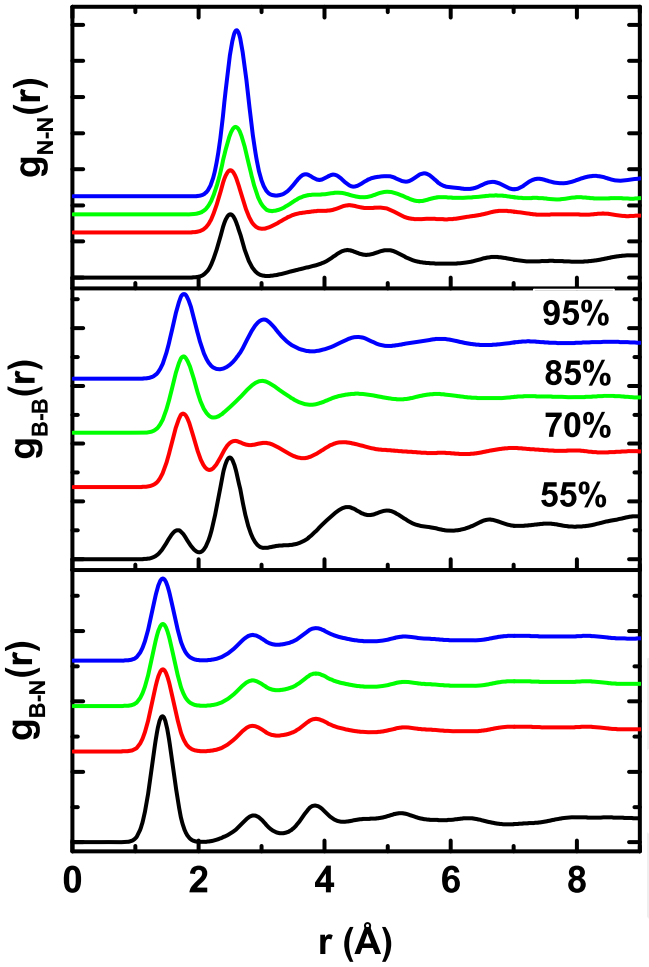

FIGURE 1 Partial pair distribution functions at some B concentrations

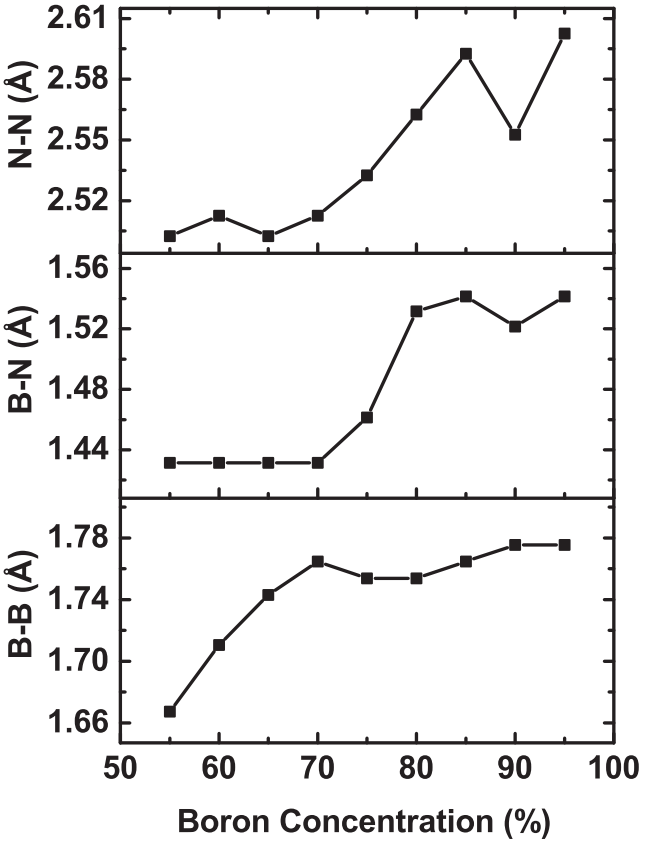

FIGURE 2 Variation in B–N, B–B and N–N separations as a function of B content

N–N distance also increases, but this increase is not too drastic (~1.2%). A visual review of the structures as shown in Figure 3 reveals that N atoms somehow prefer forming BN domains rather than being homogeneously distributed in the amorphous structures for high boron contents. Therefore, they can be classified as BN nanoscale domains in the amorphous networks. This observation can be interpreted as the occurrence of BN:B nanoscale phase separations in the models and is particularly important since it reveals that these materials can serve as nanoglass ceramics. From the PPDFs, one can also see that the models present no N-N homopolar (wrong) bonds.

Total and partial coordination numbers are estimated by using the first minimum of the PPDFs (1.94-2.05 Å for the B–N distribution and 1.96-2.27 Å for the B–B correlation depending on B contents). The N-average coordination number is around 3 up to 70 at.% B as illustrated in Figure 4, suggesting the dominated sp^2 hybridization in these amorphous alloys, in agreement with the experimental prediction.[47] At 75% B concentration, the N-coordination number rapidly rises and becomes 3.36. At this content, some of the N atoms form sp^3 hybridization. At 80% and higher B contents, most N atoms present sp^3 hybridization. This observation discloses the fact that there is a structural phase change from a 2D-like arrangement to a 3D-like arrangement in the BN-rich regions. It should be noted here that in all amorphous alloys modeled, no fivefold or higher coordinated N atoms are traced. At low B contents, the mean coordination number of B is estimated to be 3.02 and it linearly increases to 5.88 at 95% B concentration. This value is indeed comparable with the average coordination number of pure a-B. To have additional information about the microstructure of the amorphous systems, we study the coordination distribution of the models and present our findings in Figure 5. As seen from the figure, threefold-coordinated B configurations drastically decrease while sixfold coordinated B structures severally increase with increasing B content. Fourfold and fivefold coordinated arrangements initially increase, reach a maximum value at 80% B concentration and then decrease. Sevenfold coordination also forms in the models and becomes noticeable beyond 80% B content. For N atoms, the picture is very naive: there are only threefold and fourfold coordinated configurations. While one drops, the other one rises drastically between 70% and 80% concentrations.

In addition to the PPDFs and coordination number investigations, we perform the bond angle distribution analysis to

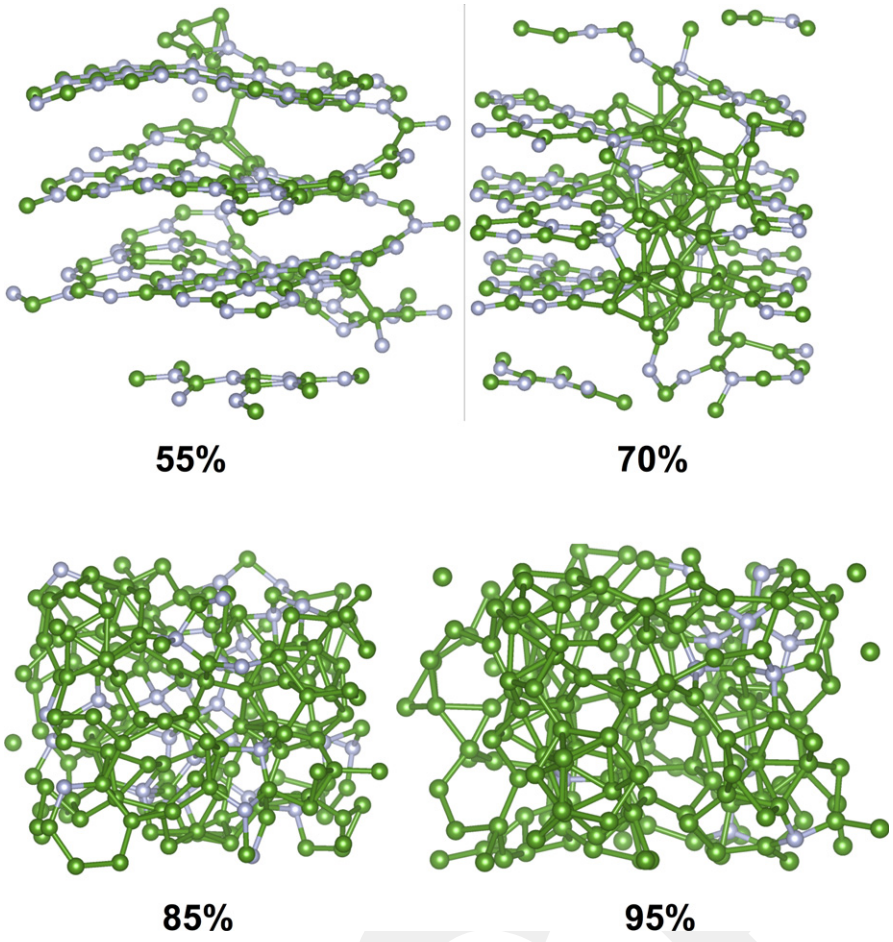

FIGURE 3 Ball stick representation of some amorphous models

have detailed information about the atomic structure of a-BNs. The B–N–B and N–B–N angle distributions of some models are shown in Figure 6. The main peak of the B–N–B and N–B–N angles is located at around 120°, suggesting the h-BN-like short-range order up to 75 at.% B at which point it shifts around 117°. At 80% B concentration, the main peak for both angle distributions is placed near 105°-111° that are pretty close to the tetrahedral angle of 109.5°, supporting a structural modification from a 2D h-BN like short-range order to a 3D c-BN or w-BN like short-range order in the BN-rich regions. When the B–B–B angles are concerned, at 55% B content it has a broad distribution ranging from 57° to 156° and has many peaks. At 60% B concentration, the distribution has two peaks at around 60° and 110° and they become stronger with increasing B content. These angles are indeed comparable with the angles of 60° and 108° originated from the intra-icosahedral bonds of the pentagonal pyramids (the quasimolecular B_{12} icosahedron). The general shape of the B-B-B angle distribution function at high B concentrations is actually quite similar to what has been reported for α-B and liquid B.

The Voronoi polyhedral approach[59] can be used to have additional information about the structures at the atomistic level. In this approach, a polyhedron is symbolized by the Voronoi index $<n_3, n_4, n_5, n_6,\ldots>$. Here, n_i and Σn_i correspond to the number of i-edge faces of polyhedron and its total coordination number, respectively. The main building unit of crystalline and a-B and B-rich materials is commonly the quasimolecular B_{12} icosahedron that consists of ideal pentagonal pyramids. The Voronoi polyhedrons with the <2,2,2,0> and <2,3,0,0> indices correspond to the ideal and defective pentagonal pyramids, respectively. Consequently, we specifically focus on them and present their variation as a function of B concentration in Figure 7. A noticeable number of these polyhedrons first appear at 60% B content and increases continuously thereafter. In order to see whether these significant amounts of ideal or defective pyramidal clusters produce any B_{12} icosahedron, we visualize the models carefully using the Vesta program and find that the first complete B_{12} molecule forms at 70% B content. In addition to the quasimolecular B_{12} icosahedron, at 75% and higher B concentrations, we discover, for the first time, the presence of a cage-like B_{16} molecule (see Figure 8) in the amorphous networks. Such a molecule has not been reported in any previous investigations. The B_{16} molecule consists of ideal pentagonal pyramids and incomplete or defective hexagonal pyramids. In the amorphous structures, each B atom of this molecule is sixfold coordinated and the B–B bond lengths range from 1.6 to 1.8 Å. We should note here that the B_{16} molecule does not

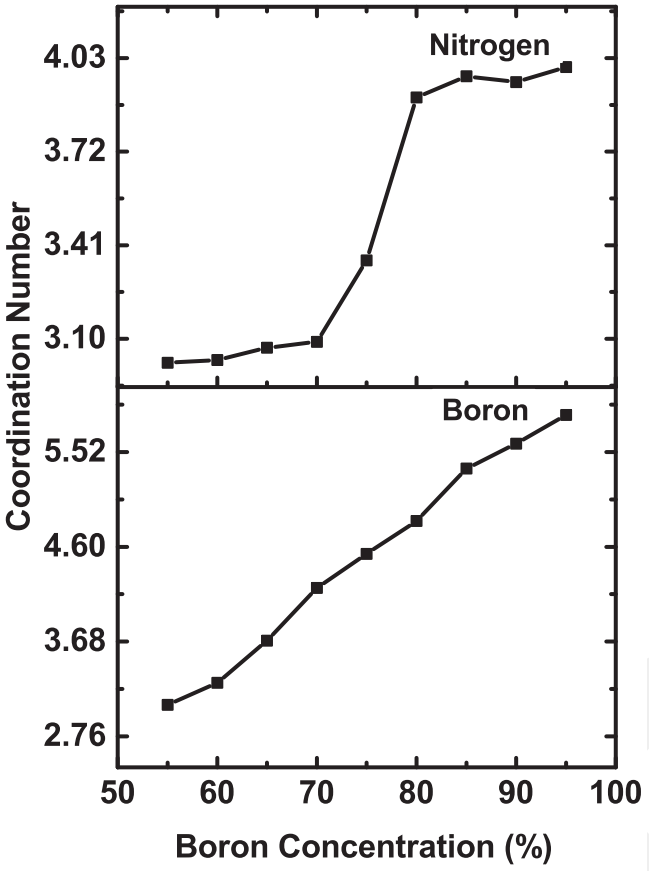

FIGURE 4 Modification of partial coordination numbers as a function of B concentration

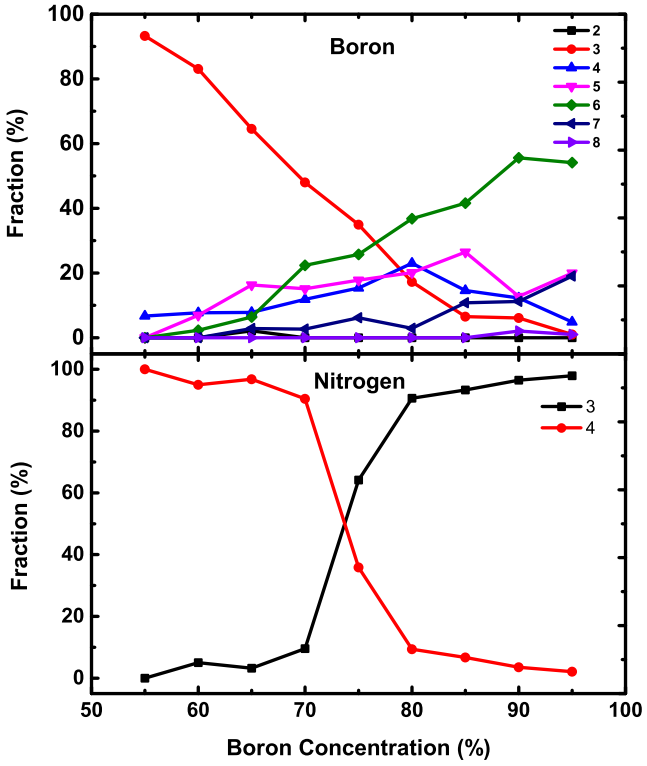

FIGURE 5 Coordination distribution of B and N atoms as a function of B concentration

develop in pure a-B model. Therefore, a kind of interaction (s) in B–N systems must be responsible for the formation of this molecule.

In order to see whether an isolated B_{16} molecule (each B atom is five-fold coordinated) is stable, we performed an additional investigation such that B_{16} cluster extracted from the amorphous network was placed in a large simulation box (breaking periodic boundary conditions) and its atomic coordinates were optimized using a conjugate gradient technique and 256 special k-points for the Brillouin zone integration. As shown in Figure 8, the cluster underwent a severe deformation and hence, we reached a conclusion that the isolated B_{16} cluster was unstable.

3.2 | Electronic properties

The crystalline and amorphous forms of BN have various high tech applications, especially in the semiconductor technology. Therefore, it is important to identify the electronic structure of the amorphous alloys proposed in this study. Figure 9 shows the modification of the HOMO-LUMO band bap energy as a function of B concentration. As understood from the figure, a 10% change in the stoichiometry results in a drastic closure of the band gap energy. Between 60% and 95% B concentrations, although the gap fluctuates, it is approaches the theoretical band gap value (0.3 eV) of a pure a-B model. It should be pointed out here that the insufficiency of the DFT-GGA approaches to describe the excited states yields an underestimation in the band gap energies. Consequently, the theoretical band gap energies are not comparable with the experimental band gaps as shown in Figure 9. Yet, in spite of the different values, one can see almost similar trend in the variation of the theoretical and experimental band gap energy[47] with changing B content (Figure 9).

3.3 | Mechanical properties

In order to predict the mechanical properties of the amorphous models, we first study their energy as a function of volume and fit the data to the third-order Birch-Murnaghan equation of states

$$E(V)=E_0+\frac{9V_0K}{16}\left\{\left[\left(\frac{V_0}{V}\right)^{\frac{2}{3}}-1\right]^3K'+\left[\left(\frac{V_0}{V}\right)^{\frac{2}{3}}-1\right]^2\left[6-4\left(\frac{V_0}{V}\right)^{\frac{2}{3}}\right]\right\} \quad (1)$$

where E (E_0) is the energy (the equilibrium energy), V (V_0) is the volume (the equilibrium volume), K is the bulk modulus at equilibrium and K' is the derivative of K with

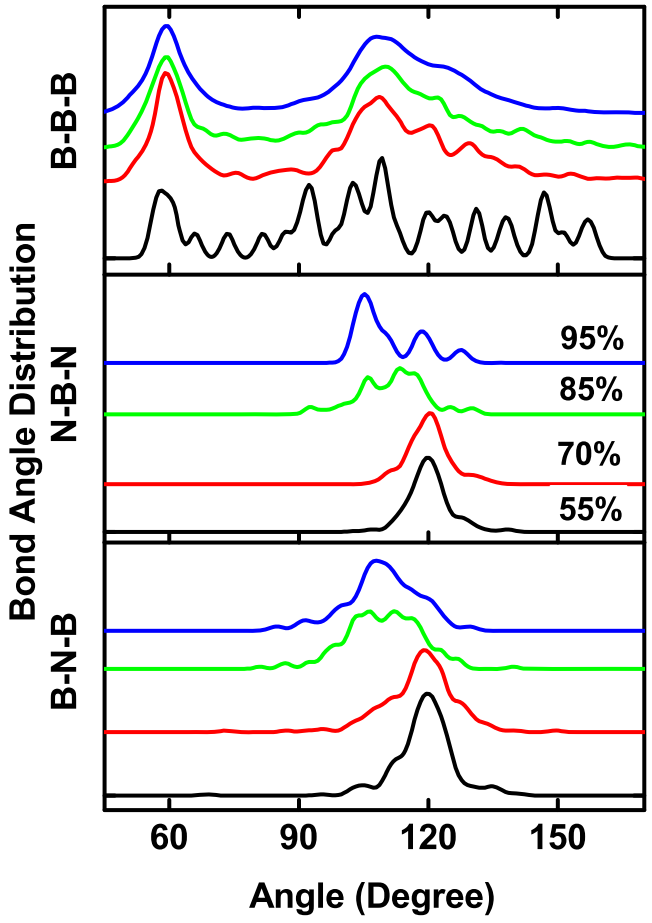

FIGURE 6 Bond angle distribution functions

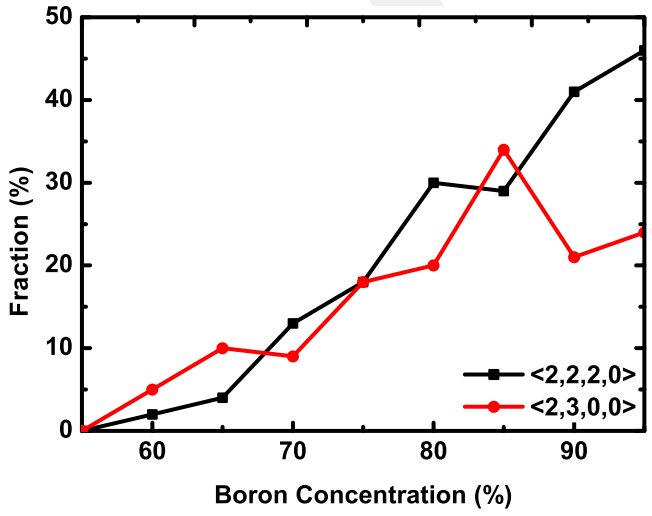

FIGURE 7 Fraction of ideal (<2,2,2,0>) and defective (<2,3,0,0>) pentagonal pyramids

respect to pressure. From the fit, we predict K (indicates the compressibility) for each material and present our data in Figure 10. The K of the network for 55 at.% B is equal to about 12 GPa, which is indeed less than the h-BN bulk modulus of ~32-36 GPa.[27,60] This might be due to the disorder nature of the models and randomly oriented hexagonal nanosheets in the amorphous networks. As expected, with increasing B content, K increases gradually and has a peak value of about 200 GPa at 80% B content, and then slightly decreases. At the peak value, the amorphous network has the largest BN domains with sp^3 hybridization, relative to the other networks. The K value of c-BN and w-BN is 390 and 375 GPa,[61,62] respectively, while it is about 200 GPa for the $B_{13}N_2$ phase[63] and the B crystals.[64-69] Consequently, the predicted K values are noticeably less than that of the 3D structured BN crystals, but they are comparable with that of B polymorphs and that of B subnitrides.

In order to calculate the Poisson's ratio, a uniaxial stress was applied along one of diagonal terms of the simulation cell vectors whereas the other stress components were set to zero. Both atomic coordinates and the simulation cell vectors were allowed to relax. The uniaxial compression generally results in an expansion in the transfer directions. This behavior is defined by the Poisson's ratio that is explained as the negative ratio of transfer strain in the i direction developing from an applied strain in the j direction,

$$\upsilon_{ij} = -\frac{\Delta L_i/L_i}{\Delta L_j/L_j}, \tag{2}$$

where L_s is the magnitude of the diagonal terms of the simulation cell vectors. The calculations were carried out in all three directions and six different values were obtained. The Poisson's ratio averaged over three directions as a function of B content is provided in Figure 10 as well. At 55% B content, it is estimated to be about 0.23, which is indeed close to 0.21 reported for h-BN.[70] As the B content is increased, the Poisson's ratio decreases linearly, as anticipated, due to the gradual structural modification from a 2D structure to a 3D structure and reaches a minimum value of 0.16. This value is fairly close to 0.15 measured for c-BN[71] and 0.11-0.13[67-69] predicted for the B polymorphs.

We can simply calculate Young's modulus (E) using the following relation:

$$E = \frac{\text{stress}}{\text{strain}} = \frac{\sigma_{ii}}{\Delta L_{ii}/L_{ii}}, \tag{3}$$

where stress and strain can be attained directly from the uniaxial compressions' simulations. Alternatively, it can be estimated using the next definition.

$$E = 3K(1 - 2\nu), \tag{4}$$

where K and ν are achieved from the Equations (1) and (2). Young's modulus computed using the both equations

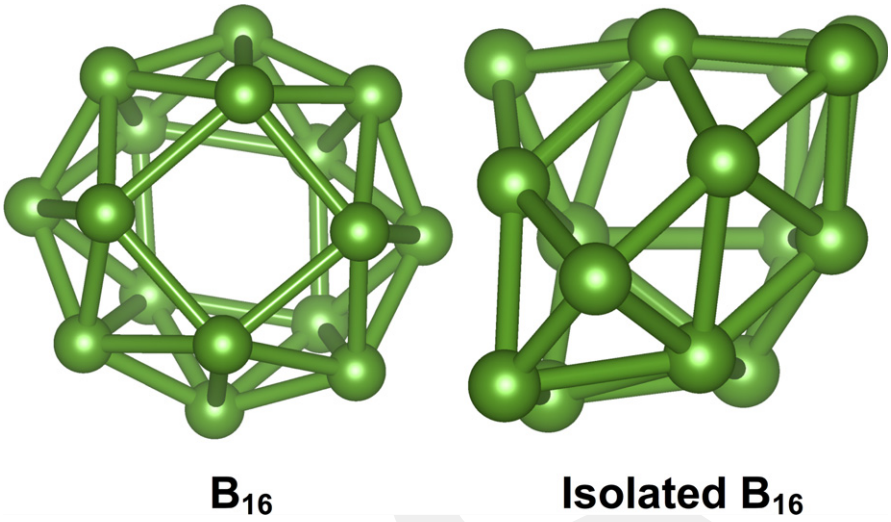

FIGURE 8 B_{16} cluster formed in the amorphous alloys and the isolated B_{16} molecule after relaxation

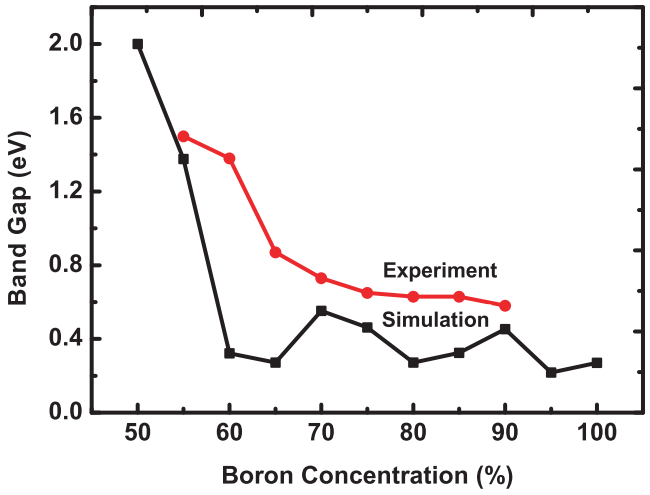

FIGURE 9 Variation in band gap energy as a function of B content. The experimental data were extracted from Ref. [48]. There are some uncertainness B contents since the experimental samples have some O and C impurities

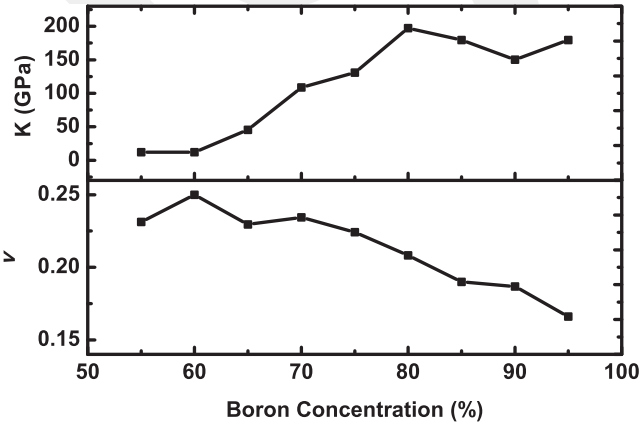

FIGURE 10 Variation in bulk modulus (K) and Poisson's ratio (υ) as a function of B content

is given in Figure 11. As seen from the figure, both approaches yield the same trend with some fluctuations. Young's modulus gradually changes from ~20 GPa to ~350 GPa. The experimental Young's modulus of a-BN:H is 47 ± 5 GPa,[72] moderately higher than our prediction for the low B contents. The value, 350 GPa estimated for high B concentrations, is noticeably smaller than 445-550 GPa found for the B crystals,[67-69] 587 ± 30 GPa estimated for the thick c-BN film,[71] 847 GPa predicted for the bulk polycrystalline material,[73] and 909 GPa reported for the single crystal c-BN.[74]

In order to estimate shear modulus (μ), we applied shear stresses on the simulation cells. After a full relaxation, we determined the shear stresses and shear strains and then calculated shear modulus using the next equation

$$\mu = \frac{\text{shear stress}}{\text{shear strain}} = \frac{\sigma_{ij}}{\frac{\Delta L_i}{L_j}} \ (i \neq j). \tag{5}$$

Alternatively shear modulus can also be projected using the following relation:

$$\mu = \frac{E}{2(1+\nu)}. \tag{6}$$

The shear modulus estimated using both equations is also provided in Figure 11 and changes from about 8.0-155 GPa. The shear modulus computed for the high B concentrations is closer to 197-236 GPa measured for the B crystals,[67-69] but it is considerably less than the shear modulus of c-BN (312-378 GPa).[73,75,76]

We finally compute the Vickers hardness using the Chen's equation[77]

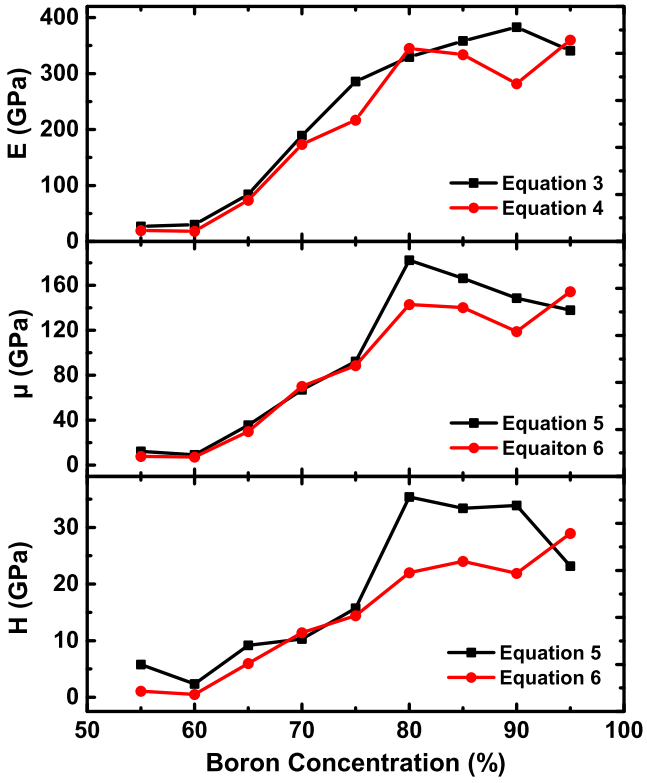

FIGURE 11 Young's Modulus (E), Shear modulus (μ) and Vickers hardness (*H*) as a function of B content. Shear moduli obtained using Equations (5) and (6) are used to estimate the Vickers hardness

$$H = 2\left(\frac{\mu}{n^2}\right)^{0.585} - 3(\text{GPa}), \tag{7}$$

where μ is the shear modulus and n is the Pugh ratio ($n = K/\mu$). The variation in the hardness shown in Figure 11 reveals that at 80% and higher B concentrations, the Vickers hardness is greater than 20 GPa, implying that these amorphous alloys can be considered as a hard material. Yet the hardness values estimated are less than ~40 GPa projected for B crystals.[78]

4 | DISCUSSION

Our simulations expose some remarkable features of the B-rich a-BN materials. The first interesting observation is the occurrence of BN:B phase separations in these networks. Even at low boron concentrations, the model mainly has h-BN-like structure and the excess B atoms are aggregated to one side of the model and produce B-rich region(s), as illustrated in Figure 3. The excess B atoms principally connect randomly distributed and oriented h-BN like nanosheets to form a 3D-like structure. The observation of such phase separations is actually quite important because it proposes that these systems can serve as nanoglass materials.

We also observe the occurrence of a 2D-to-3D phase transformation in the BN-rich regions by simply changing B concentration. Such a structural phase transformation meaningfully improves the mechanical properties of the amorphous networks (Figures 9and 10). The Vickers hardness of some alloys reaches a value larger than 20 GPa, offering that they have potential to serve as hard materials. Yet we need to underline here that due to the linear fitting, we do definitely expect some errors in our predicted Poisson's ratios, Young's moduli and shear moduli and hence the Vickers hardness. Careful experimental studies are indeed desirable to reveal their accurate mechanical properties.

Another interesting finding is the formation of a small cage like B_{16} molecule that does not exist in pure a-B. Consequently, we believe that interaction of B-N atoms is responsible for the formation of the B_{16} molecule. Although the isolated B_{16} molecule (each B atoms is five-fold coordinated) is found to be not stable ie it undergoes a drastic deformation, it might be stabilize by functionalizing it with some elements or molecules. Therefore, further investigations are certainly needed to provide more information about this simple molecule and its properties. Additionally at present, we do not know whether the B_{16} molecule is unique for only B–N systems or it can also form in other B-rich amorphous materials such BC, BSi etc. Therefore, further studies are absolutely desirable to shed some light onto this issue.

Experimental investigations have applied the plasma chemical vapor deposition, ion-beam deposition, spin coating process, etc. to produce B-rich a-BN films. Yet in these studies,[46-48] possible B:BN phase separations have not been discussed. It is likely that these techniques did not allow the formation of such separations or the samples had such phase separations, but they might be too small to be clearly identified by the current experimental techniques. Here, we will suggest the traditional experimental technique to manufacture B-rich a-BN alloys having B:BN phase separations such that they can serve as *nanoglass* ceramics. As mentioned above, there exist several B-rich BN crystalline phases such as $B_{13}N_2$, $B_{50}N_2$, B_6N, etc. They are generally prepared from B/BN melts at high-temperature and pressure conditions. At very high temperatures, B-rich BN systems are known to form mixtures of phases of B and BN, signifying that the observation of the phase separations in the present work is physical. We believe that the same experimental procedure can be applied to fabricate the B-rich amorphous materials with phase separations if and only if significantly fast quenching rates are applied to suppress the crystallization. Note that depending on quenching rates, different structured amorphous materials having different size of amorphous or amorphous-crystalline domains for the same composition can be prepared. Additionally,

the application of pressure to the melts can drop the 2D-to-3D phase modification to lower B concentrations such that the materials can have larger BN domains having sp^3 hybridization. Controlling the size of domains in the amorphous alloys and their local structure can have significant impacts on their electronic structure (band gap engineering) and mechanical properties. Therefore, these materials can offer a wide range of applications in semiconductor technology.

Finally we need to stress here that all these findings are based on the 216 atoms amorphous models. For real systems, macroscopic phase separations can take place instead of nanoseparations, the 2D-to-3D phase transformation in the BN-rich regions can occur at a different B content, and the formation of a complete quasimolecular B_{12} icosahedron can form at a distinct B concentration. Therefore, for real systems all properties of these amorphous alloys can differ from the estimated ones in this study.

5 | CONCLUSIONS

We have generated, for the first time, B-rich a-B_xN_{1-x} ($0.55 \leq x \leq 0.95$) models using ab initio MD simulations and recovered their local structure, mechanical properties, and electronic structures. As perceived in B/BN melts, we notice clear BN:B phase separations in all amorphous networks. This observation means that these amorphous materials can serve as *nanoglass* ceramics. Two types of hybridizations are observed in the BN-rich domains depending on B concentration. Below 70 at.% B, sp^2 hybridization is dominated and the short-range order of the amorphous networks is similar to that of the 2D h-BN structure. The sp^2 and sp^3 hybridizations form between 70 at.% B and 80 at.% B. At higher B concentrations, sp^3 hybridization with a frequency of ~90%-98% is perceived in the amorphous configurations as seen in the c-BN or w-BN crystals. Consequently, a phase transformation from the 2D structure to the 3D structure in the BN-rich domains is proposed. In the B-rich regions, we find that 60% B concentration is significant enough to produce the ideal and defective pentagonal pyramids and 70% B content is adequate to observe a complete B_{12} molecule. In addition to the B_{12} molecule, the formation of a cage-like B_{16} molecule is, for the first time, observed in some amorphous alloys. Yet we find that the isolated B_{16} molecule is not stable. Some of these B-rich amorphous materials possess a high Vickers harness and hence they can be used as hard materials. The electronic structure calculations suggest that all amorphous materials are semiconductor. We also speculate that B-rich BN *nanoglasses* can be synthesized from fast quenching of B/BN melts.

ACKNOWLEDGMENTS

This work was supported by the Scientific and Technological Research Council of Turkey (TÜBİTAK) under grant number 114C100. The simulations were run on the TÜBİTAK ULAKBİM, High Performance and Grid Computing Center (TRUBA resources).

ORCID

Murat Durandurdu http://orcid.org/0000-0001-5636-3183

REFERENCES

1. Williams DS. Elastic stiffness and thermal expansion coefficient of boron nitride films. *J Appl Phys*. 1985;57:2340-2342.
2. Trice RW, Halloran JW. Investigation of the physical and mechanical properties of hot-pressed boron nitride/oxide ceramic composites. *J Eur Ceram Soc*. 1999;82:2563-2565.
3. Watanebe K, Taniguchi T, Kanda H. Direct-bandgap properties and evidence for ultraviolet lasing of hexagonal boron nitride single crystal. *Nat Mater*. 2004;3:404-409.
4. Lei W, Zhang H, Wu Y, et al. Oxygen-doped boron nitride nanosheets with excellent performance in hydrogen storage. *Nano Energy*. 2014;6:219-224.
5. Mcgregor DS, Unruh TC, Mcneil WJ. Thermal neutron detection with pyrolytic boron nitride. *Nucl Instr Meth Phys Res*. 2008;591:530-533.
6. Zheng M, Liu Y, Wang P, et al. Synthesis and formation mechanism of cubic boron nitride nanorods in lithium bromide molten salt. *Mater Lett*. 2013;91:206-208.
7. Mohammad SN. Electrical characteristics of thin film cubic boron nitride. *Solid-State Electron*. 2002;46:203-222.
8. Obodo KO, Andrew RC, Chetty N. Modification of the band offset in boronitrene. *Phys Rev B*. 2011;84:155308.
9. Eichler J, Lesniak C. Boron nitride (BN) and BN composites for high-temperature applications. *J Eur Ceram Soc*. 2008;28:1105-1109.
10. Taniguchi T, Teraji T, Koizumi S, et al. Appearance of n-type semiconducting properties of cBN single crystals grown at high pressure. *Jpn J Appl Phys*. 2002;41:L109.
11. King SW, French M, Bielefeld J, et al. X-ray photoelectron spectroscopy investigation of the Schottky barrier at a-BN: H/Cu interfaces. *Electrochem Solid-State Lett*. 2011;14:H478-H479.
12. Caruso AN. The physics of solid-state neutron detector materials and geometries. *J Phys: Condens Matter* 2010;22:443201.
13. Kurakevych OO, Solozhenko VL. High-pressure design of advanced BN-based materials. *Molecules*. 2016;21:1399-1414.
14. Loh KP, Gamo MN, Sakaguchi I. Thermal stability of the negative electron affinity condition on cubic boron nitride. *Appl Phys Lett*. 1998;72:3023-3025.
15. Britnell L, Gorbachev R, Jalil R, et al. Electron tunneling through ultrathin boron nitride crystalline barriers. *Nano Lett*. 2012;12:1707-1710.
16. Akinwande D, Petrone N, Hone J. Two-dimensional flexible nanoelectronics. *Nat Commun*. 2014;5:5678.

17. Balmain WH. Bemerkungen über die Bildung von Verbindungen des Bors und Siliciums mit Stickstoff und gewissen Metallen. *J Prakt Chem*. 1842;27:422-430.
18. Matsui Y, Sekikawa Y, Sato T, et al. Formations of rhombohedral boron nitride, as revealed by TEM-electron energy loss spectroscopy. *J Mater Sci*. 1981;16:1114-1116.
19. Wentorf RH Jr. Synthesis of the cubic form of boron nitride. *J Chem Phys*. 1961;34:809-812.
20. Bundy FP, Wentorf RH Jr. Direct transformation of hexagonal boron nitride to denser forms. *J Chem Phys*. 1963;38:1144-1149.
21. Levitas VI, Hashemi J, Ma YZ. Strain-induced disorder and phase transformation in hexagonal boron nitride under quasi-homogeneous pressure: in situ X-ray study in a rotational diamond anvil cell. *Europhys Lett*. 2004;68:550.
22. Corrigan FR, Bundy FP. Direct transitions among the allotropic forms of boron nitride at high pressures and temperatures. *J Chem Phys*. 1975;63:3812-3820.
23. Britun VF, Kurdyumov AV. Mechanisms of martensitic transformations in boron nitride and conditions of their development. *High Press Res*. 2000;17:101-111.
24. Taniguchi T, Sato T, Utsumi W, et al. Effect of nonhydrostaticity on the pressure induced phase transformation of rhombohedral boron nitride. *Appl Phys Lett*. 1997;70:2392-2394.
25. Ji C, Levitas VI, Zhu H, et al. Shear-induced phase transition of nanocrystalline hexagonal boron nitride to wurtzitic structure at room temperature and lower pressure. *J Superhard Mater*. 2012;109:19108-19112.
26. Dubrovinskaia N, Solozhenko VL, Miyajima N, et al. Superhard nanocomposite of dense polymorphs of boron nitride: noncarbon material has reached diamond hardness. *Appl Phys Lett*. 2007;90:101912.
27. Solozhenko VL, Will G, Elf F. Isothermal compression of hexagonal graphite-like boron nitride up to 12 GPa. *Solid State Commun*. 1995;96:1-3.
28. Levitas VI, Ma Y, Hashemi J, et al. Strain-induced disorder, phase transformations, and transformation-induced plasticity in hexagonal boron nitride under compression and shear in a rotational diamond anvil cell: in situ X-ray diffraction study and modeling. *J Chem Phys*. 2006;125:044507.
29. Meng Y, Mao HK, Eng PT, et al. The formation of sp^3 bonding in compressed BN. *Nat Mater*. 2004;3:111.
30. Dub SN, Petrusha IA. Mechanical properties of polycrystalline cBN obtained from pyrolytic gBN by direct transformation technique. *High Press Res*. 2006;26:71-77.
31. Taniguchi T, Sato T, Utsumi W, et al. In-situ X-ray observation of phase transformation of rhombohedral boron nitride under static high pressure and high temperature. *Diamond Relat Mater*. 1997;6:1806-1815.
32. Lorenz H, Orgzall I. Influence of the initial crystallinity on the high pressure–high temperature phase transition in boron nitride. *Acta Mater*. 2004;52:1909-1916.
33. Britun VF, Kurdyumov AV, Borimchuk NI, et al. Formation of diamond-like BN phases under shock compression of graphite-like BN with different degree of structural ordering. *Diamond Relat Mater*. 2007;16:267-276.
34. Nistor LC, Van TG, Dinca G. Crystallographic aspects related to the high pressure–high temperature phase transformation of boron nitride. *Philos Mag*. 2005;85:1145-1158.
35. Kurdyumov AV, Britun VF, Petrusha IA. Structural mechanisms of rhombohedral BN transformations into diamond-like phases. *Diamond Relat Mater*. 1996;5:1229-1235.
36. Becker R, Avci R, Murusidze I, et al. Metallic boron nitride. *Eur Chem Bull*. 2015;4:8-23.
37. Condon JB, Holcombe CE, Johnson DH, et al. The kinetics of the boron plus nitrogen reaction. *Inorg Chem*. 1976;15:2173-2179.
38. Solozhenko VL, Kurakevych OO. New boron subnitride B13N2: HP-HT synthesis, structure and equation of state. *J Phys Conf Ser*. 2008;121:1-7.
39. Solozhenko VL, Kurakevych OO. Chemical interaction in the B-BN system at high pressures and temperatures: synthesis of novel boron subnitrides. *J Solid State Chem*. 2009;182:1359-1364.
40. Guo J, Wang H, Zhu MK, et al. Synthesis of B 50 N 2 nanorods by electrolysis of organic solutions. *Electrochem Commun*. 2006;8:1211-1214.
41. Hubert H, Garvie LAJ, Buseck PR, et al. High-pressure, high-temperature syntheses in the B-C–N–O system. *J. Solid-State Chem*. 1997;133:356-364.
42. Solozhenko VL, LE GODEC Y, Kurakevych OO. Solid-state synthesis of boron subnitride, B 6 N: myth or reality?. *C R Acad Sci Ser II C: Chim*. 2006;9:1472-1475.
43. Zedlitz R, Heintze M, Schubert MB. Properties of amorphous boron nitride thin films. *J Non-Cryst Solids*. 1996;198:403-406.
44. Huang JY, Yasuda H, Mori H. HRTEM and EELS studies on the amorphization of hexagonal boron nitride induced by ball milling. *J Am Ceram Soc*. 2000;83:403-409.
45. Durandurdu M. Hexagonal nanosheets in amorphous BN: a first principles study. *J Non-Cryst Solids*. 2015;427:41-45.
46. Kho JG, Moon KT, Nouet G, et al. Boron-rich boron nitride (BN) films prepared by a single spin-coating process of a polymeric precursor. *Thin Solid Films*. 2001;389:78-83.
47. Ong CW, Chan KF, Choy CL. Optical absorption and transport mechanisms of dual ion-beam-deposited boron-rich boron nitride films. *Thin Solid Films*. 2001;388:217-225.
48. Pouch JJ, Alterovitz SA, Miyoshi K, et al. Boron nitride: composition, optical properties, and mechanical behavior. *Mater Res Soc Symp Proc*. 1987;93:1-2.
49. Ordejón P, Artacho E, Soler JM. Self-consistent order-N density-functional calculations for very large systems. *Phys Rev B*. 1996;53:R10441-R10444.
50. Becke AD. Density-functional exchange-energy approximation with correct asymptotic behavior. *Phys Rev A*. 1988;38:3098-3100.
51. Lee C, Yang W, Parr RG. Development of the Colle-Salvetti correlation-energy formula into a functional of the electron density. *Phys Rev B*. 1988;37:785-789.
52. Troullier N, Martins JL. Efficient pseudopotentials for plane-wave calculations. *Phys Rev B*. 1991;43:1993-2006.
53. Parrinello M, Rahman A. Polymorphic transitions in single crystals: a new molecular dynamics method. *J Appl Phys*. 1981;52:7182-7190.
54. Momma K, Izumi F. VESTA 3 for three-dimensional visualization of crystal, volumetric and morphology data. *J Appl Crystallogr*. 2011;44:1272-1276.
55. Le Roux S, Petkov V. ISAACS–interactive structure analysis of amorphous and crystalline systems. *J Appl Crystallogr*. 2010;43:181-185.

56. Kumashiro Y. *Electric Refractory Materials*. New York: Taylor & Francis; 2000.
57. Delaplane RG, Lundstrom T, Dahlborg U, et al. AIP Conf. Proc. No. 231. AIP. New York. 1991; pp. 241.
58. Krishnan S, Ansell S, Felten JJ, et al. Price, structure of liquid boron. *Phys Rev Lett*. 1998;81:586.
59. Medvedev NN. EDVEDEV. The algorithm for three-dimensional Voronoi polyhedra. *J Comput Phys*. 1986;67:223-229.
60. Solozhenko VL, Peun T. Compression and thermal expansion of hexagonal graphite-like boron nitride up to 7 GPa and 1800 K. *J Phys Chem Solids*. 1997;58:1321-1323.
61. Datchi F, Dewaele A, Godec YL, et al. Equation of state of cubic boron nitride at high pressures and temperatures. *Phys Rev B*. 2007;75:214104.
62. Solozhenko VL, Häusermann D, Mezouar M, et al. Equation of state of wurtzitic boron nitride to 66 GPa. *Appl Phys Lett*. 1998;72:1691-1693.
63. Kurakevych OO, Godec YL, Solozhenko VL. Equations of state of novel solids synthesized under extreme pressure–temperature conditions. *J Phys Conf Ser*. 2015;653:1-6.
64. Lyakhov AO, Oganov AR. Evolutionary search for superhard materials: methodology and applications to forms of carbon and TiO_2. *Phys Rev B*. 2011;84:092103.
65. Zarechnaya EY, Dubrovinsky L, Dubrovinskaia N, et al. Superhard semiconducting optically transparent high pressure phase of boron. *Phys Rev Lett*. 2009;102:185501-185503.
66. Nelmes RJ, Loveday JS, Allan DR, et al. Neutron-and X-ray-diffraction measurements of the bulk modulus of boron. *Phys Rev Lett*. 1993;47:7668.
67. Jiang C, Lin Z, Zhang J, et al. First-principles prediction of mechanical properties of gamma-boron. *Appl Phys Lett*. 2009;94:191906.
68. Aydın S, Simsek M. First-principles calculations of elemental crystalline boron phases under high pressure: orthorhombic B 28 and tetragonal B 48. *J Alloys Compd*. 2011;509:5219-5229.
69. Qin J, Nishiyama N, Ohfuji H, et al. Polycrystalline γ-boron: as hard as polycrystalline cubic boron nitride. *Scripta Mater*. 2012;67:257-260.
70. Peng Q, Ji W, De S. Mechanical properties of the hexagonal boron nitride monolayer: ab initio study. *Comput Mater Sci*. 2012;56:11-17.
71. Zhang F, Guo Y, Song Z, et al. Deposition of high quality cubic boron nitride films on nickel substrates. *J Appl Phys Lett*. 1994;65:971-973.
72. King SW, French M, Bielefeld J, et al. Valence band offset at the amorphous hydrogenated boron nitride-silicon (100) interface. *Appl Phys Lett*. 2012;101:042903-042905.
73. Manghnani MH. Proceedings of the 5th NIRIM International Symposium on Advanced Material (ISAM'98) Tsukuba, Japan. 1998;73.
74. Grimsditch M, Zouboulis ES, Polian A. Elastic constants of boron nitride. *J Appl Phys*. 1994;76:832-834.
75. Wang SQ, Ye HQ. First principles study on elastic properties and phase stability of III–V compounds. *Phys Status Solid B*. 2003;240:45-54.
76. Daoud S, Loucif K, Bioud N, et al. First-principles study of structural, elastic and mechanical properties of zinc-blende boron nitride (B3-BN). *Acta Phys Pol, A*. 2012;122:1.
77. Chen XQ, Niu H, Li D, et al. Modeling hardness of polycrystalline materials and bulk metallic glasses. *Intermetallics*. 2011;19:1275-1281.
78. Oganov AR, Solozhenko VL, Gatti C, et al. The high-pressure phase of boron, γ-B28: disputes and conclusions of 5 years after discovery. *J Superhard Mater*. 2011;33:363-379.

How to cite this article: Çetin AÖ, Durandurdu M. Hard boron rich boron nitride nanoglasses. *J Am Ceram Soc*. 2017;00:1–11. https://doi.org/10.1111/jace.15383